J|A|C|S ARTICLES

Published on Web 07/06/2009

Probing Conformers and Adsorption Footprints at the Single-Molecule Level in a Highly Organized Amino Acid Assembly of (*S*)-Proline on Cu(110)

Matthew Forster,[†] Matthew S. Dyer,[†] Mats Persson,[†,‡] and Rasmita Raval*[,†]

Surface Science Research Centre and Department of Chemistry, University of Liverpool, Liverpool, L69 3BX, U.K., and Department of Applied Physics, Chalmers University of Technology, SE-412 96, Göteborg, Sweden

Received March 24, 2009; E-mail: R.Raval@liv.ac.uk

Abstract: Establishing the nanoscale details of organized amino acid assemblies at surfaces is a major challenge in the field of organic−inorganic interfaces. Here, we show that the dense (4 × 2) overlayer of the amino acid, (*S*)-proline on a Cu(110) surface can be explored at the single-molecule level by scanning tunneling microscopy (STM), reflection absorption infrared spectroscopy (RAIRS), and periodic density functional theory (DFT) calculations. The combination of experiment and theory, allied with the unique structural rigidity of proline, enables the individual conformers and adsorption footprints adopted within the organized assembly to be determined. Periodic DFT calculations find two energetically favorable molecular conformations, projecting mirror-image chiral adsorption footprints at the surface. These two forms can be experimentally distinguished since the positioning of the amino group within the pyrrolidine ring leads each chiral footprint and associated conformer to adopt very different ring orientations, producing distinct contrasts in the STM images. DFT modeling shows that the two conformers can generate eight possible (4 × 2) overlayers with a variety of adsorption footprint arrangements. STM images simulated for each structural model enables a direct comparison to be made with the experiment and narrows the (4 × 2) overlayer to one specific structural model in which the juxtaposition of molecules leads to the formation of one-dimensional hydrogen bonded prolate chains directed along the [1$\bar{1}$0] direction.

1. Introduction

The nanoscale control of biomolecular self-organization at inorganic interfaces is an important stepping stone toward realizing nanotechnological applications in sensors,[1] enantioselective catalysis,[2] molecular electronics,[3] tailored biomineralization, and molecular nanodevices.[4] In all these cases, the biologically relevant molecules implant complex, responsive, and selective functions to surfaces. Within this context, the behavior of single monolayers of amino acids at metal surfaces has attracted attention over the past decade.[5−15] Of particular interest is the ability of amino acids to self-organize on surfaces leading to the creation of local nanoscale assemblies,[7] one-dimensional strings,[4a,8] and highly organized arrays that cover macroscopic length scales.[6a,9] Specifically, the uniform interfaces created by the extended, ordered, two-dimensional structures[9−11,14] are highly attractive for technological applications and as models of molecular assembly in two dimensions.

However, determining the nanoscale details of extended amino acid assemblies has proved to be a major challenge in the field. Three aspects contribute to this: first, the range of chemical forms that can be adopted; second, the multiple points of interaction that are available to optimise molecule−substrate interactions; third, intermolecular interactions, e.g., hydrogen bonding, which often provide the driving force for organization. This complexity is exemplified by investigations of the organized (3 × 2) adlayers of glycine[11−13] and alanine[12,14,15] on Cu(110). This work has extracted information on the chemical nature of the adsorbed amino acid, the possible orientations adopted, identified the bonding interactions with the surface, and suggested the types of local adsorption footprints that could be adopted.[14a,b,15] Despite this level of information, producing a definitive description of the organized structure remains a

[†] University of Liverpool.
[‡] Chalmers University of Technology.

(1) (a) Rosi, N. L.; Mirkin, C. A. *Chem. Rev.* **2005**, *105*, 1547. (b) Cao, Y. W. C.; Jin, R.; Mirkin, C. A. *Science* **2002**, *297*, 1536.
(2) Izumi, Y. *Adv. Catal.* **1983**, *32*, 215.
(3) (a) Joachim, C.; Gimzewski, J. K.; Aviram, A. *Nature* **2000**, *408*, 541. (b) Heath, R. J.; Keukes, P. J.; Snider, G. S.; Williams, R. S. *Science* **1998**, *280*, 1716.
(4) (a) Schiffrin, A.; Riemann, A.; Auwarter, W.; Pannec, Y.; Weber-Bargioni, A.; Cvetko, D.; Cossaro, A.; Morgante, A.; Barth, J. V. *Proc. Natl. Acad. Sci. U.S.A.* **2007**, *104*, 5279. (b) Bumm, L. A.; Arnold, J. J.; Cygan, M. T.; Dunbar, T. D.; Burgin, T. P.; Jones, L., II; Allara, D. L.; Tour, J. M.; Weiss, P. S. *Science* **1996**, *271*, 1705. (c) Romaner, L.; Heimel, G.; Gruber, M.; Bredas, J.-L.; Zojer, E. *Small* **2006**, *2*, 1468. (d) Heimel, G.; Romaner, L.; Bredas, J.-L.; Zojer, E. *Surf. Sci.* **2006**, *600*, 4548.
(5) Mateo Marti, E.; Barlow, S. M.; Haq, S.; Raval, R. *Surf. Sci.* **2002**, *501*, 191.
(6) (a) Zhao, X.; Yan, H.; Zhao, R. G.; Yang, W. S. *Langmuir* **2003**, *19*, 809. (b) Humblot, V.; Mthivier, C.; Pradier, C. M. *Langmuir* **2006**, *22*, 3089. (c) Zhao, X.; Gai, Z.; Zhao, R. G.; Yang, W. S.; Sakurai, T. *Surf. Sci.* **1999**, *424*, L347. (d) Zhao, X.; Zhao, R. G.; Yang, W. S. *Surf. Sci.* **1999**, *442*, L995. (e) Iwai, H.; Tobisawa, M.; Emori, A.; Egawa, C. *Surf. Sci.* **2005**, *574*, 214. (f) Jones, T. E.; Baddeley, C. J.; Gerbi, A.; Savio, L.; Rocca, M.; Vattuone, L. *Langmuir* **2005**, *21*, 9468. (g) Feyer, V.; Plekan, O.; Skala, T.; Chab, V.; Matolin, V.; Prince, K. *J. Phys. Chem. B* **2008**, *112*, 13655.

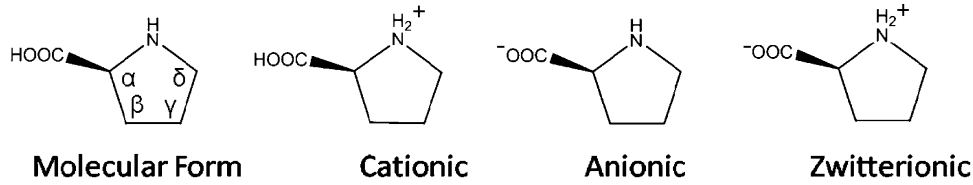

Figure 1. The structure and chemical forms of (*S*)-proline. The four inequivalent CH ring positions are labeled α to δ.

challenge since a multiplicity of arrangements can be suggested by theory, and there is no easy way to verify which one prevails under the experimental conditions.

The general challenges of applying DFT calculations to amino acid overlayers are outlined in ref 16. For example, periodic DFT calculations of enantiopure alanine on Cu(110) suggest that five possible structures with near identical heats of adsorption could potentially be created.[14b] Determining which structure actually exists has not been possible because averaging techniques like reflection absorption infrared spectroscopy (RAIRS) and NEXAFS do not provide information at the single-molecule level, while nanoscale probing by scanning tunneling microscopy (STM) is unable to resolve the issue since all the adsorbates image similarly, and there is insufficient contrast to allow discrimination between the various conformers and their adsorption footprints.

In order to address this general problem of structure determination in organized amino acid adlayers, we turned to proline, an amino acid in which the amino group is incorporated within the pyrrolidine ring, Figure 1, leading to a unique structural rigidity. This causes the bonding configuration of the NH group to trigger significant concomitant reorientation of the attached pyrrolidine ring when the amino acids adopt distinct conformers with different adsorption footprints at a surface. Such pyrrolidine reorientations should lead to image contrasts that would act as a marker flag of local adsorption footprints and local molecular geometry and, thus, enable a molecule-by-molecule analysis of the organized assembly.

Here we combine STM and RAIRS experiments on the (4 × 2) assembly of (*S*)-proline on Cu(110)[5] with periodic DFT calculations, complemented by STM and RAIRS simulations, in order to arrive at a definitive structure that identifies the positions and adsorption footprints occupied by coexisting conformers. This represents a real step-change in unraveling the complex structures that are formed by amino acids at well-defined metal surfaces.

2. Experimental and Theoretical Methods

The Cu(110) surface was prepared by argon ion sputtering at 500 eV followed by annealing to 800 K and showed an average terrace size of 800 Å. Low energy electron diffraction (LEED) was utilized to check the cleanliness of the sample, with a sharp (1 × 1) pattern characteristic of clean Cu(110). (*S*)-proline (99%) was purchased from Sigma-Aldrich and dosed from an electrically heated glass tube, separated from the main chamber by a gate valve and differentially pumped by a turbomolecular pump. The sample was thoroughly outgassed to ensure sample purity prior to dosing. In all experiments the Cu(110) crystal was held at room temperature during dosing.

STM images were recorded, at room temperature, in an ultrahigh vacuum (UHV) chamber, with a base pressure of 2×10^{-10} mbar, and fitted with a Specs Aarhus 150 STM operated in constant current mode with an electrochemically etched tungsten tip. The bias voltage was applied to the sample.

RAIRS experiments were performed in a multitechnique UHV chamber interfaced a Mattson 6020 FTIR spectrometer via ancillary optics and KBr windows. A nitrogen-cooled HgCdTe detector allowed the spectral range of 650−4000 cm^{-1} to be accessed. The resolution of the spectrometer was set to 4 cm^{-1} and 250 scans were coadded. The spectrum of the clean sample was taken as a background reference, R^0, at the beginning of the experiments. Spectra of the adsorbed layer were then obtained during continuous dosing of proline, with the crystal at room temperature, and are displayed as the ratio $(R - R^0)/R^0$ with respect to the clean sample spectrum.

Calculations were carried out using the VASP periodic density functional theory (DFT) package.[17] Plane waves were used as a basis set with an energy cutoff of 400 eV. Valence electron−core interactions were included using the projector augmented wave method,[18] and the generalized gradient approximation was used for the exchange-correlation functional.[19] The Cu(110) surface was included as a six-layer slab. Calculations of isolated prolate anions on this surface were carried out in a supercell corresponding to a (4 × 4) surface unit cell and a total height of 20.6 Å and were performed on a 4 × 3 × 1 *k*-point grid. Calculations of the (4 × 2) arrangements were carried out in a smaller supercell containing two anions in a (4 × 2) surface unit cell but with the same height and were performed on a 4 × 6 × 1 *k*-point grid.

In every case, geometry relaxation was performed on the prolate anions and the top three copper layers until the force on every atom was smaller than 0.01 eV/Å. Corrections were made to the energy and electrostatic potential to compensate for periodic images of the dipole moment in the *z*-direction. In-line with other amino acids on the Cu(110) surface,[6b,11,14] proline is dehydrogenated upon

(7) (a) Kuhnle, A.; Linderoth, T. R.; Besenbacher, F. *J. Am. Chem. Soc.* **2003**, *125*, 14680. (b) Kuhnle, A.; Linderoth, T. R.; Hammer, B.; Besenbacher, F. *Nature* **2002**, *415*, 891.
(8) Lingenfelder, M.; Tomba, G.; Constantini, G.; Ciacchi, L. C.; De Vita, A.; Kern, K. *Angew. Chem., Int. Ed.* **2007**, *46*, 4492.
(9) Barlow, S. M.; Louafi, S.; Le Roux, D.; Williams, J.; Muryn, C.; Haq, S.; Raval, R. *Langmuir* **2004**, *20*, 7171.
(10) (a) Barlow, S. M.; Raval, R. *Surf. Sci. Rep.* **2003**, *50*, 201. (b) Barlow, S. M.; Raval, R. *Curr. Opin. Colloid Interface Sci.* **2008**, *13*, 65.
(11) (a) Barlow, S. M.; Kitching, K. J.; Haq, S.; Richardson, N. V. *Surf. Sci.* **1998**, *401*, 322. (b) Booth, N. A.; Woodruff, D. P.; Schaff, O.; Giessel, T.; Lindsay, R.; Baumgartel, P.; Bradshaw, A. M. *Surf. Sci.* **1998**, *397*, 258. (c) Kang, J.-H.; Toomes, R. L.; Polcik, M.; Kittel, M.; Hoeft, J.-T.; Efstathiou, V.; Woodruff, D. P.; Bradshaw, A. M. *J. Chem. Phys.* **2003**, *118*, 6059.
(12) Rankin, R. B.; Sholl, D. S. *J. Phys. Chem. B* **2005**, *109*, 16764.
(13) (a) Nyberg, M.; Odelius, M.; Nilsson, A.; Pettersson, L. G. M. *J. Chem. Phys.* **2003**, *119*, 12577. (b) Blankenburg, S.; Schmidt, W. G. *Nanotechnology* **2007**, *18*, 424030.
(14) (a) Barlow, S. M.; Louafi, S.; Le Roux, D.; Williams, J.; Muryn, C.; Haq, S.; Raval, R. *Surf. Sci.* **2005**, *590*, 243. (b) Jones, G.; Jones, L. B.; Thibault-Starzyk, F.; Seddon, E. A.; Raval, R.; Jenkins, S. J.; Held, G. *Surf. Sci.* **2006**, *600*, 1924. (c) Sayago, D. I.; Polcik, M.; Nisbet, G.; Lamont, C. L. A.; Woodruff, D. P. *Surf. Sci.* **2005**, *590*, 76. (d) Haq, S.; Massey, A.; Moslemzadeh, N.; Robin, A.; Barlow, S. M.; Raval, R. *Langmuir* **2007**, *23*, 10694. (e) Williams, J.; Haq, S.; Raval, R. *Surf. Sci.* **1996**, *368*, 303.
(15) Rankin, R. B.; Sholl, D. S. *Surf. Sci.* **2004**, *548*, 301.
(16) James, J. N.; Sholl, D. S. *Curr. Opin. Colloid Interface Sci.* **2008**, *13*, 60.
(17) Kresse, G.; Furthmüller, J. *Phys. Rev. B* **1996**, *54*, 11169.
(18) Kresse, G.; Joubert, J. *Phys. Rev. B* **1999**, *59*, 1758.
(19) Perdew, J. P.; Wang, Y. *Phys. Rev. B* **1992**, *45*, 13244.

adsorption. Despite the fact that the adsorbed species is formally anionic, the calculations were performed in a cell without an overall charge. Charging occurs by transfer of electrons from the metal surface to the dehydrogenated proline molecule. Following geometry relaxation, the adsorption energy was calculated in the (4 × 4) supercell by comparing to the energies of a hydrogen atom adsorbed at the short bridge site, a proline molecule in vacuum, and a clean copper surface calculated in the same supercell.

Constant current STM images were simulated in the Tersoff−Hamann approximation,[20] by plotting contours of constant integrated local density of states (LDOS) from the Fermi energy to the bias potential. It is not possible to obtain absolute values of the tunneling currents at a given tip−surface height using the Tersoff−Hamann approximation, so the LDOS plots in this study are shown with an average tip−surface distance of 7.5 Å. This is large enough to avoid the region in which there would be a chemical interaction between the tip and the sample, which is not included in this method. Increasing the tip−surface distance up to an average of 10 Å does not produce qualitative changes of the images.

The normal modes for the adsorbed species were calculated in the harmonic approximation. In the calculation of the normal modes, the top layer of the copper surface was included in addition to the prolate anions, with the remaining copper atoms kept fixed. At the same time, the change in the dipole moment in the *z*-direction was calculated for each mode and used to simulate the results of RAIRS experiments.

3. Results and Discussion

3.1. The Chemical Forms of Proline. Proline is a unique amino acid in that the amino functionality is contained within a five-membered ring. This leads to increased structural rigidity, and thus the number of possible conformers is greatly reduced compared to other amino acids. Gas-phase conformers of proline are divided into two groups depending upon the orientation of the carboxylic acid and amino functionalities with respect to the plane of the pyrrolidine ring. The cis conformation is adopted when the carboxylate group occupies the same side of the ring as the amino group, while the trans conformation is adopted when they occupy opposite sides of the ring. The pyrrolidine ring contains four inequivalent CH environments labeled α to δ, Figure 1. The crystal structure of proline reveals that the pyrrolidine ring is almost planar, with the δ carbon out of plane by approximately 0.6 Å.[21]

Proline can exist in four possible chemical forms: neutral, cationic, anionic, and zwitterionic (Figure 1). The chemical nature of the molecule is heavily dependent upon the immediate environment. The zwitterionic form is favored in the crystalline state and in solution near the isoelectric point. The anionic and cationic forms are pH dependent, favored by basic and acidic solutions, respectively. The neutral molecular form is adopted by gas-phase molecules. The chemical form adopted by proline at surfaces has also been shown to be heavily dependent upon the local environment, with the zwitterionic form favored on TiO_2[22] and Pd(111) surfaces,[23] in contrast to the anionic species favored on Cu(110).[5]

Proline plays an active role in the folding of proteins and peptides where its steric effects influence the stability and position of the protein folds.[24] (*S*)-Proline and its derivatives have also been implicated in diastereoselective heterogeneous catalysis, helping to stereodirect reaction pathways.[25]

3.2. The (4 × 2) Molecular Assembly of (*S*)-Proline on Cu(110). Previous RAIRS and LEED studies by our group have shown that the adsorption of (*S*)-proline on Cu(110) at 300 K leads directly to a (4 × 2) overlayer.[5] Weak LEED spots appear at the lowest exposures, becoming sharper upon increasing coverage, indicating an island growth mechanism. The RAIRS studies[5] indicated that the (4 × 2) adlayer consists of the prolate species in which the carboxylic acid group has dehydrogenated to give a carboxylate functionality that facilitates bonding to the surface, as also observed for a number of other amino acids.[6b,11,14] Qualitative application of the metal surface selection rules for RAIRS suggested that the pyrrolidine ring is orientated largely parallel to the surface and that the plane of the carboxylate is tilted significantly toward the surface plane. Thus, a molecular assembly consisting of a repeat one-molecule (4 × 2) unit mesh was suggested.[5] Thermal desorption studies further demonstrated that this phase is stable until around 500 K,[5] highlighting the robust nature of this molecular assembly and its ability to survive at elevated temperatures.

STM data presented here provide a more detailed description of this biomolecular assembly. First, STM images clearly confirm the island growth mechanism, showing that small islands with (4 × 2) periodicity are created at the earliest stages of adsorption, with increasing exposure leading to large islands that are elongated in the $[1\bar{1}0]$ direction, Figure 2a. Increasing coverage to create a saturated monolayer leads to coalescence of these islands, with antiphase domain boundaries created in the process, Figures 2b and 2c. Finally, further exposure leads to the formation of multilayers (not shown).

Two important aspects emerge from our STM data. Whereas the previous LEED studies were not able to provide any information on the nature of the (4 × 2) unit mesh, the high resolution STM images confirm that there is an additional molecule accommodated in the center, Figure 2d, yielding an overall two-molecule unit cell. Second, this central molecule is imaged weaker at all the voltage conditions used, while the corner molecules remained bright, leading to an apparent height difference of approximately 0.4 Å, Figure 2e. This observation suggests that the (4 × 2) molecular assembly consists of two distinct prolate molecules. Finally, the STM images show that local defect unit meshes do occur in which all the molecules are identical and image as either all weak or all bright, Figure 2f and 2g, respectively, suggesting that the primitive (4 × 2) unit cell with two inequivalent molecules enjoys only a slight energetic advantage compared to the centered (4 × 2) unit mesh where all molecules are equivalent.

Overall, the (4 × 2) prolate assembly is very similar to the (3 × 2) overlayers of alaninate and glycinate on Cu(110), with the larger unit mesh of the (4 × 2) phase arising from the increased molecular dimensions of prolate due to the incorporation of the amino group within the pyrrolidine cycle. STM and LEED experiments carried out with the mirror (*R*)-proline enantiomer on Cu(110) also yield the same (4 × 2) organization,

(20) Tersoff, J.; Hamann, D. R. *Phys. Rev. Lett.* **1983**, *50*, 1998.
(21) Kayushina, R. L.; Vainshtein, B. K. *Sov. Phys. Crystallogr.* **1996**, *10*, 698.
(22) (a) Fleming, G. J.; Idriss, H. *Langmuir* **2004**, *20*, 7540. (b) Fleming, G. J.; Adib, K.; Rodriguez, J. A.; Barteau, M. A.; White, J. M.; Idriss, H. *Surf. Sci.* **2008**, *602*, 2029. (c) Fleming, G. J.; Adib, K.; Rodriguez, J. A.; Barteau, M. A.; Idriss, H. *Surf. Sci.* **2007**, *601*, 5726.
(23) (a) Goa, F.; Wang, Y.; Tysoe, W. T. *J. Chem. Phys. C* **2008**, *112*, 6145. (b) Goa, F.; Wang, Y.; Burkholder, L.; Tysoe, W. T. *Surf. Sci.* **2007**, *601*, 3579.
(24) Sapse, A. M.; Mallah-Levy, L.; Daniels, S. B.; Erickson, B. W. *J. Am. Chem. Soc.* **1987**, *109*, 3526.
(25) (a) Besson, M.; Blanc, B.; Champelet, M.; Gallezot, P.; Nasar, K.; Pinel, C. *J. Catal.* **1997**, *170*, 254. (b) Ranade, V. S.; Consilglio, G.; Prins, R. *Catal. Lett.* **1999**, *58*, 71.

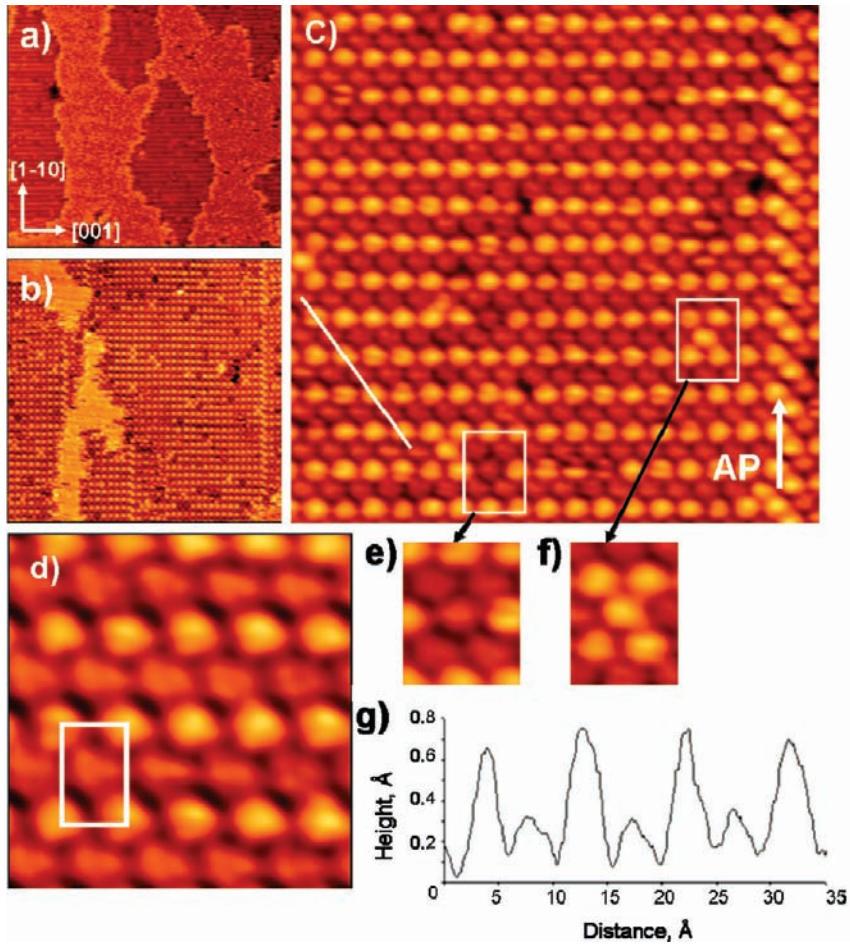

Figure 2. (a) STM image (451 Å × 420 Å^2, $I_t = -0.34$ nA, $V_t = -1250$ mV) showing low coverage island growth of the (4 × 2) phase. The surface directions are the same for all subsequent images within this figure. (b and c) STM images showing (4 × 2) islands joining together at increasing coverage with the creation of antiphase boundaries, indicated in c as AP (132 Å × 128 Å^2, $I_t = -0.52$ nA, $V_t = -1583$ mV and 140 × 128 Å^2, $I_t = -0.40$ nA, $V_t = -806$ mV, respectively). (d) High resolution STM image with the (4 × 2) unit indicated (37 × 39 Å^2, $I_t = -0.47$ nA, $V_t = -423$ mV). (e) Diagonal line scan (indicated on c) showing the height contrast within the overlayer. (f and g) Expansion STM images from c showing defect unit meshes containing all 'weak' or all 'bright' molecules, respectively.

which is what would be expected from symmetry considerations. For the sake of simplicity, the discussion from this point will focus only the adsorption of enantiopure (*S*)-proline on Cu(110).

3.3. Bonding, Orientation, and Footprint Chirality of the Isolated Adsorbed Prolate Species. In order to gain a better understanding of the (4 × 2) molecular assembly, DFT calculations were carried out for an isolated adsorbed prolate species in a (4 × 4) unit cell in order to minimize interactions with molecules in neighboring unit cells. Although an exhaustive search of all possible adsorption sites and geometries was too computationally expensive, geometry relaxations were performed from several starting geometries leading to the three low energy structures shown in Figure 3, whose calculated adsorption energies are shown in Table 1. Structures A and B possess the highest adsorption energies and are preferred over Structure C. Both A and B are adsorbed with the two oxygen atoms on neighboring copper atoms along a close-packed row and the nitrogen atom on a copper atom in the next row, in agreement with the known adsorption geometries of other amino acids on the same surface.[6b,11,14] The two oxygen atoms of the carboxylate and the nitrogen atom of the amino group essentially provide a three-point bonding interaction of the prolate with the substrate, and thus the adsorption geometry can be defined in terms of its adsorption footprint, as shown in Figure 3. Specifically, the triangular footprints projected by structures A and B are chiral and represent nonsuperimposable mirror images as they are confined in two dimensions and thus unable to flip over. Importantly, the chirality of the adsorption footprint leads to a concomitant reorientation of the pyrrolidine ring. Thus, the more stable structure A, with its left-handed triangular footprint, has its ring tilted away from the surface whereas structure B, which describes a right-handed triangular footprint, possesses a flat-lying ring and is less stable by just 30 meV.

We note that *footprint chirality* should not be confused with *molecular chirality*. A clear distinction has been given by Barlow et al.[10a] for adsorption of chiral molecules at surfaces, which essentially dissects local adsorption motifs in terms of the configuration of the inherent chiral center within the adsorbed species and the chirality of the adsorption footprint. Thus, enantiopure adlayers of amino acids possess *molecular homochirality* but can project different footprints, leading to *footprint heterochirality*. Footprint chirality is a central issue in the discussion of amino acid organization at surfaces since it directly reflects the optimum molecule−metal bonding contacts made by individual molecules in an assembly. Footprint chirality also determines the overall 2-D arrangements of the outward-facing side chains that will determine the assembly's response to its environment. In systems such as glycine[11] and alanine[14] on Cu(110), a large body of experimental literature

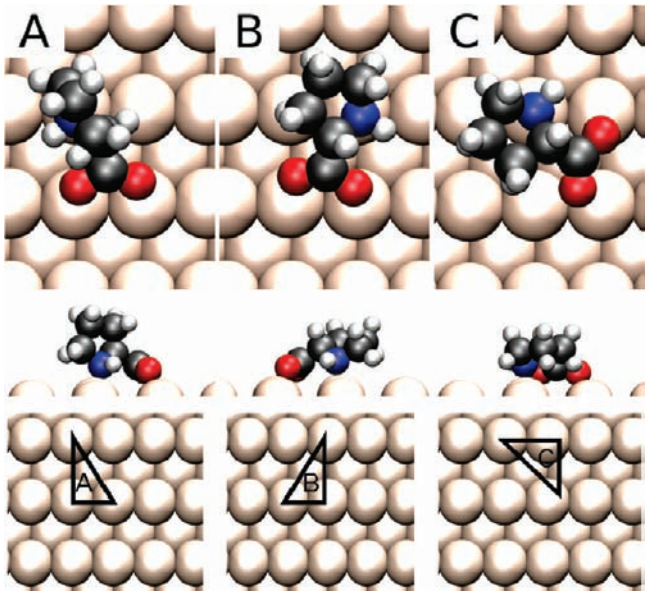

Figure 3. Relaxed adsorption geometries for the three most stable isolated prolate anions in a (4 × 4) unit cell on Cu(110). First Row: shown from above. Second Row: along the close-packed [1$\bar{1}$0] rows. Third Row: the molecular adsorption footprint. Color code: Red (oxygen), blue (nitrogen), black (carbon), white (hydrogen).

Table 1. Adsorption Energies of Prolate Anion in a (4 × 4) Unit Cell on Cu(110)

structure	A	B	C
E_{ads} (eV/molecule)	1.23	1.20	1.13

has been dedicated to the characterization of the molecular species and their general orientation. A parallel body of theoretical work has taken the discussion further and analyzed detailed adsorption geometries, the bonding interactions with the surfaces, and the resulting adsorption footprints that can be adopted.[12,14b,15] A major question in the field is whether an entire assembly adopts the same triangular footprint (footprint homochirality) or whether both mirror forms of the triangular footprints are adopted (footprint heterochirality). Calculations by Rankin and Sholl[12,15] on the adsorption of enantiopure alanine and glycine on Cu(110) find a preference for (3 × 2) organizations constructed from homochiral molecules with heterochiral footprints. A later calculation by Jones and coworkers of the alanine/Cu(110) system[14b] also favors five closely related heterochiral footprint structures. Monte Carlo simulations of alanine on Cu(110)[26] show that the evolution of organization and local patterns within these systems is strongly influenced by the adsorption footprints the system adopts. So far, direct experimental verification of which footprints are adopted in an assembly does not exist. In the next section, we see that the rigid structure of the prolate provides a good marker of this information.

3.4. The (4 × 2) Molecular Assembly: Bonding, Conformers and Adsorption Footprints. (i) Energetics of Different Assemblies. STM images, Figure 2, show that the (4 × 2) assembly possesses a two-molecule repeat unit, comprising two distinct species which image differently. This is consistent with a unit mesh containing prolate species in two of the calculated adsorption geometries shown in Figure 3. As geometry C has the lowest adsorption energy and, furthermore, cannot easily be accommodated with another molecule in a (4 × 2) unit cell, it has been discounted. This leaves eight distinct arrangements in which prolate species with adsorption geometries A and/or B are placed in the (4 × 2) unit cell. The relaxed geometries of the eight arrangements are shown in Figure 4, along with their corresponding adsorption footprints. The computed adsorption energy for each arrangement is shown in Table 2. It can be seen from Table 2 that arrangements II, III, IV, and VII can be ruled out on energetic grounds. However, this still leaves four other arrangements (I, V, VI, VIII) as potential candidates for the (4 × 2) structure, and despite their distinct structural makeup, distinguishing between them entirely on calculated energetic grounds alone is rather difficult.

(ii) Distinguishing between the Various Assemblies: STM Simulations. In order to extend our understanding of amino acid assembly further, we embarked on establishing other characteristics that could be put to the test both experimentally and theoretically. Hence, simulated STM images were calculated for all eight arrangements, Figure 5, to allow direct comparison with experiment. It is apparent that only the arrangements containing both adsorption geometries A and B give rise to two spots with different heights in a unit cell. Therefore, arrangements containing only one type of adsorption geometry (either all A or all B) can be discounted. Of the arrangements affording the correct imaging contrast, only arrangements I and VI yield STM images which are in good agreement with experiments collected at the same bias. However, arrangement I is energetically less favorable than arrangements V and VIII, which offer STM simulations in poor agreement with experiment, and is therefore discounted. This leaves arrangement VI, which possesses the highest adsorption energy of all the possible (4 × 2) arrangements and, furthermore, yields an STM image which is in very good agreement with experiment, as shown in Figure 6. The relative positions of the prolate species with respect to the imaged features in the simulated STM image are shown in Figure 6a along with the experimental STM image for comparison, Figure 6b. It can be seen from these that the STM data discriminates remarkably well between the two coexisting conformers adopted by the prolate in Structure VI, with brighter spots imaged above the ring of the upright molecules (A) and the fainter spots above the nitrogen atom in the flat-lying molecules (B). Thus, the conformations and the adsorption footprints adopted within the (4 × 2) assembly can be identified directly at the single-molecule level.

This unique molecule-by-molecule STM insight into the individual conformations adopted within the amino acid assembly is a direct consequence of the structural rigidity of the prolate and the fact that the adsorption footprints adopted by conformations A and B are mirror images, differing only in the copper atom upon which the nitrogen occupies, yielding left- and right-handed right-angled triangles. In geometry B the nitrogen lies to the right, with respect to the carboxylate, which allows the ring to lie flat, and so this conformer is imaged fainter. However, if the nitrogen lies to the left with respect to the carboxylate, the ring is forced to tilt significantly away from the surface and images brighter; this is what happens for conformation A. As a result, one obtains a detailed insight into the nanoscale construction of the (4 × 2) phase and can narrow the structure to arrangement VI which comprises homochiral molecules with heterochiral adsorption footprints associated with two different conformers.

(26) Unac, R. C.; Gil Rabaza, A. V.; Vidales, A. M.; Zgrablich, G. *Appl. Surf. Sci.* **2007**, *254*, 125.

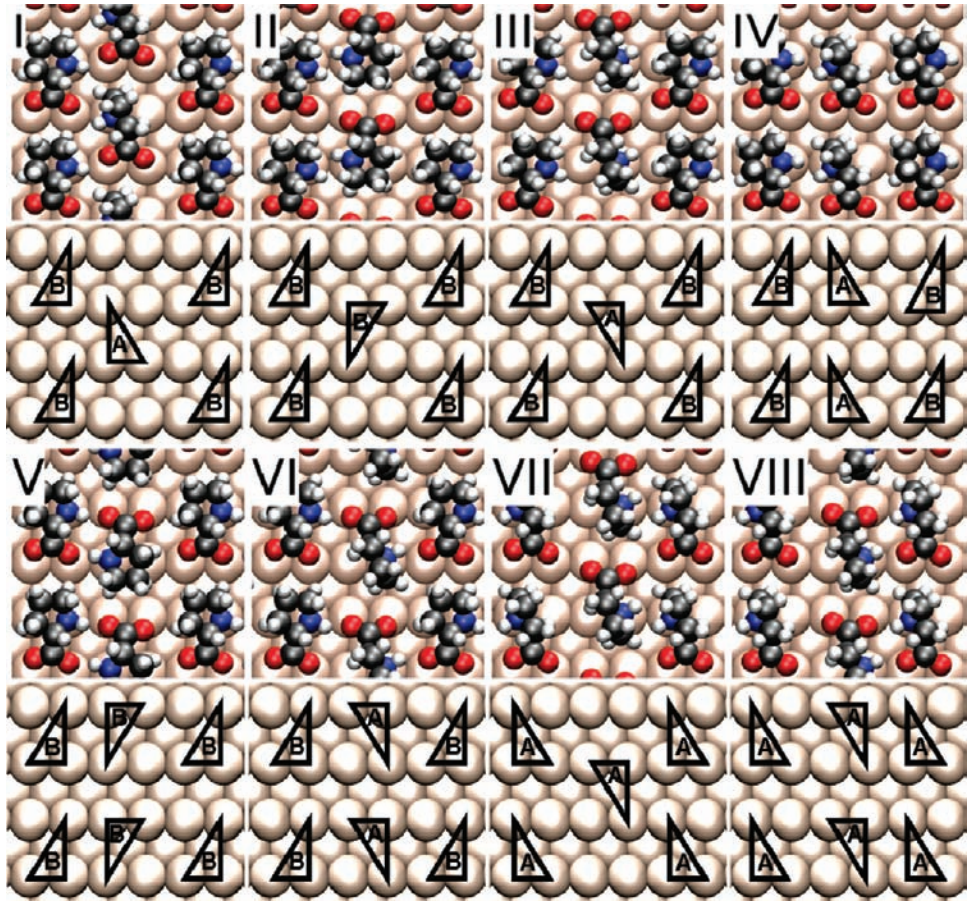

Figure 4. Relaxed adsorption geometries for the eight calculated (4 × 2) arrangements of prolate anions on Cu(110) (the first and third rows) with the corresponding molecular footprint geometry indicated (the second and fourth rows). Color code for atoms is as in Figure 3.

Table 2. Adsorption Energies of (4 × 2) Arrangements of Prolate Anions on Cu(110)[a]

arrangement	I (A+B)	II (B+B)	III (A+B)	IV (A+B)	V (B+B)	VI (A+B)	VII (A+A)	VIII (A+A)
E_{ads} (eV/molecule)	1.25	0.95	1.15	0.99	1.32	1.38	1.09	1.29

[a] The energy for arrangement VI was calculated in a (4 × 4) super-cell and the energies of the other arrangements calculated from their energies relative to structure VI in a (4 × 2) super-cell. The two adsorption geometries (A or B) contained within each arrangement are also stated.

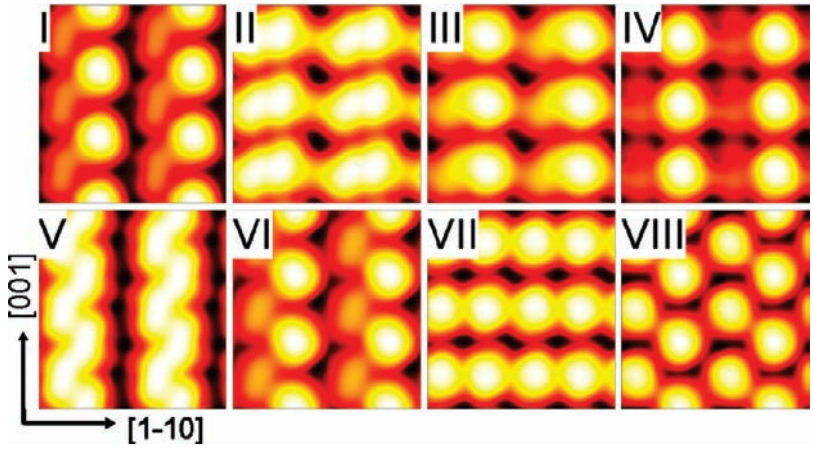

Figure 5. Calculated STM images of the eight (4 × 2) arrangements. Images are shown in an (8 × 6) surface unit cell and are simulated at a bias voltage of −1.25 V with an average tip−surface height of 7.5 Å.

A significant contribution to the high stability of arrangement VI may be attributed to intermolecular hydrogen bonding, although we note that simply 'counting hydrogen bonds' in dense amino acid structures is not an absolute measure of the relative stability of various structures in DFT calculations.[27] Arrangement VI allows for each adsorbed anion to participate in two distinct N···H···O bonds as shown in Figure 7. The N···H···O distances of 2.82 Å and 3.01 Å and angles of 146°

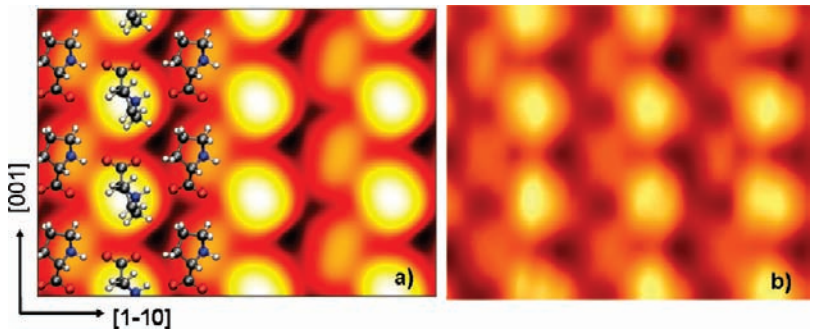

Figure 6. (a) Simulated STM image; the positions of the atoms in the prolate anions are included. The calculated image is shown in a (12 × 6) unit cell under the same conditions as Figure 5. (b) High resolution STM image of (4 × 2) phase (31.1 × 21.7 Å^2, $I_t = -0.43$ nA, $V_t = -1250$ mV).

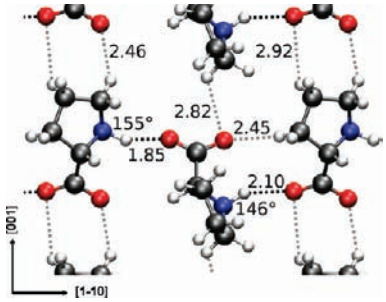

Figure 7. Hydrogen bonding chains in arrangement VI (surface directions are indicated). Strong and weak hydrogen bonds are shown with black and gray dashed lines respectively. Bond lengths (Å) and angles (deg) are indicated, and the color code is as in Figure 3.

and 155° lie within the values expected for a moderately strong hydrogen bond. In addition the increase in the calculated N···H bond distance to 1.034 Å for prolate molecules in arrangement IV compared to 1.031 Å for an isolated adsorbed molecule A and 1.026 Å for an isolated adsorbed molecule B also suggests the formation of hydrogen bonds.[28] Hydrogen bonding between adjacent molecules in the [1$\bar{1}$0] direction leads to the creation of one-dimensional hydrogen bonded proline chains. This helps to rationalize the experimental observation that (4 × 2) islands are elongated in the [1$\bar{1}$0] direction. The minimum calculated distance of 2.46 Å between the carboxylate oxygen and the hydrogen of a CH_2 group in adjacent prolate molecules in the [001] direction would only allow for the formation of weak hydrogen bonds in this direction,[28] thus preventing the creation of a strongly hydrogen bonded 2D network. Other intermolecular interactions such as dipole−dipole and surface-mediated interactions may provide additional binding between neighboring molecules. As a result of all intermolecular interactions, the adsorption energy per molecule for arrangement VI is 0.15 eV higher than for an isolated adsorbed molecule with structure A, the most stable isolated anion.

(iii) RAIRS Data of the (4 × 2) Assembly: Theory and Experiment. The vibrational bands recorded in our previous RAIRS study of the prolate (4 × 2) system[5] were analyzed within a single-species adsorption model and assigned on the basis of literature values obtained for proline-based organometallic complexes[29] and for the isolated proline molecule.[30]

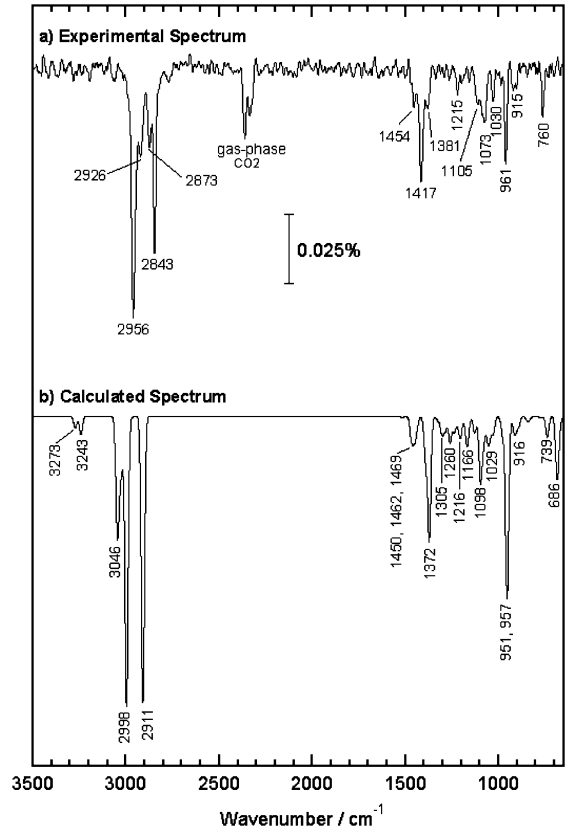

Figure 8. (a) Experimental RAIR spectrum for high coverage (*S*)-proline on Cu(110) at 300 K. (b) Calculated RAIRS spectrum of arrangement VI (major peaks indicated).

However, the presence of two different conformers shown by this study needs to be taken into account, as has the fact that adsorption of proline onto an extended copper surface is likely to alter the vibrational frequencies and dipole moments considerably. To address this issue, DFT calculations of the normal modes of vibration generated by arrangement VI were undertaken and compared directly with the experimental RAIR spectrum, Figure 8. The overall spectral pattern and the major peaks in the experimental spectrum are all reproduced in the calculation with good agreement. We note that DFT calculated normal-mode frequencies are only accurate within an average error of ∼50 cm^{-1},[31] so an exact match with experiment is not expected. Furthermore, the calculations are based on the

(27) Rankin, R. B.; Sholl, D. S. *Langmuir* **2006**, *22*, 8096.
(28) Desiraju, G. R.; Steiner, T. *The Weak Hydrogen Bond*; Oxford Univ. Press: Cary, NC, 1999.
(29) Herlinger, A. W.; Long, T. V. *J. Am. Chem. Soc.* **1970**, *4*, 6481.
(30) Reva, I. D.; Stepanian, S. G.; Plokhotnichenko, A. M.; Radchenko, E. D.; Sheina, G. G.; Blagoi, Yu. P. *J. Mol. Struct.* **1994**, *318*, 1.
(31) Riley, K. E.; Op't Holt, B. T.; Merz, K. M. *J. Chem. Theory Comput.* **2007**, *3*, 407.

Table 3. Comparison of Frequencies for the Experimental and Calculated RAIR Spectrum and Corresponding Assignments (vibrations arising from geometries A and B are indicated)[a]

	calculated RAIR spectrum		
experimental RAIR spectrum, frequency (cm^{-1})	frequency, (cm^{-1})	absolute intensity ($D^2/Å^2/amu$)	description of the normal modes (and associated conformer)
2956 (s)	3046	0.18	B: $C_\beta H_2$ and $C_\gamma H_2$ as str
2926 (sh)	2998	0.57	A: $C_\beta H_2$ and $C_\gamma H_2$ s str
2873 (sh)			
2843 (s)	2911	0.50	B: $C_\alpha H$ str and $C_\delta H_2$ s str
1454 (sh)	1469	0.04	A and B: CH_2 sciss
	1462	0.02	A and B: CH_2 sciss
	1450	0.04	A: CH_2 sciss
1417 (m)	1393	0.08	A and B: COO^- s str and NH ip bend
1381 (sh)	1372	0.24	A & B: COO^- s str & NH ip bend
	1305	0.03	B: NH ip bend and CH_x def
1215 (w)	1216	0.01	B: NH ip bend and CH_x def
1105 (sh)	1098	0.13	A: NH op bend and CH_2 wag
1073 (m)			
1030 (w)	1029	0.03	B: CH_x def and ring mode
961 (m)	957	0.24	A: ring mode
	951	0.13	B: COO^- sciss and ring mode
915 (w)	916	0.02	B: CH_x def, ring mode & COO^- sciss
760 (m)	739	0.04	A and B: and COO^- sciss and ring mode
	686	0.12	B: COO^- sciss and ring mode

[a] The carbon atoms are labeled α to δ according to Figure 1, the conformer as in Figure 3. Key: Str, stretch; as, asymmetric stretch; s, symmetric stretch; sciss, scissors; CH_x def, deformations (comprising wag, twist, rock, and bending modes); ip, in-plane; op, out-of-plane; s, strong; m, medium; w, weak; sh, shoulder.

harmonic approximation and so do not account for combination/overtone bands and Fermi resonance phenomena that can complicate the CH stretching region. Nevertheless, a number of comparisons can be made as follows. Table 3 compares the experimental RAIR spectrum with the calculated spectrum and the description of the normal modes giving rise to the vibrational bands. A list of the calculated frequencies, absolute RAIRS intensities, and description of the 70 normal modes possessing frequencies higher than 600 cm^{-1} can be found in the Supporting Information. The major spectral regions of interest are described in more detail below.

The CH_2 Stretching Region. The CH_2 stretching region of the proline molecule is particularly rich since the methylene groups are largely uncoupled, with vibrational amplitudes localized within specific CH_2 groups. The bands at 2956 and 2926 cm^{-1} are attributed to the $C_\beta H_2$ and $C_\gamma H_2$ groups, with observable vibrations dictated by the ring orientations adopted in the two conformers. Thus, observable intensities arise from the asymmetric $C_\beta H_2$ and $C_\gamma H_2$ stretches of the flat-lying B conformers, whereas it is the symmetric $C_\beta H_2$ and $C_\gamma H_2$ stretches that are observable from the tilted A conformer. The flat-lying B conformer also gives rise to a strong band at 2843 cm^{-1}, which possesses a strong contribution from the stretching vibration of the upward pointing $C_\alpha H$ group.

The Carboxylate Stretches. The $\nu_s COO^-$ symmetric stretch of the carboxylate group is reproduced, with the calculated value of 1393 and 1372 cm^{-1} comparing well with the experimentally observed peaks at 1417 and 1381 cm^{-1}. The attenuation of this normally intense band suggests the carboxylate plane is tilted significantly away from the normal, which is the case for both prolate conformers. Furthermore, the absence of the corresponding asymmetric $\nu_{as} COO^-$ confirms that the bonding oxygen atoms are equidistant from the surface.

The NH Bends. The NH bond lies largely parallel to the surface for both A and B conformations. This orientation is supported by the medium intensity out-of-plane NH bend contribution at 1098 cm^{-1} in the simulated spectrum. This vibration was originally assigned to the 961 cm^{-1} peak;[5] however, on the basis of our calculations, we reassign the out-of-plane NH bend + CH_2 wag to the experimentally observed band at 1073 cm^{-1}, with the upshift in frequency possibly arising from the close proximity and coupling of the NH group to the surface. The 961 cm^{-1} band is now assigned to a mixed COO^- scissors and ring mode.

Finally, the calculated spectrum reproduces the major spectral features in the low wavenumber region. However, we note that a number of these lower frequency vibrations show significant intermixing and contain contributions from a range of molecular vibrations, making an absolute assignment of each vibrational band challenging.

4. Conclusions

In conclusion, we show that the individual conformers and adsorption footprints adopted within the highly organized (4 × 2) amino acid assembly of (*S*)-prolate on Cu(110) can be identified at the single-molecule level. STM images and periodic DFT calculations of this phase clearly show that two distinct prolate conformers, possessing mirror-image chiral adsorption footprints, are energetically favored. The two conformers are distinguishable in the STM images since the rigidity of proline, derived from the placement of the amino group within the pyrrolidine ring, triggers a major reorientation of the ring as the chirality of the adsorption footprint is altered. Eight possible (4 × 2) arrangements were considered on energetic grounds. STM simulations generated for each arrangement allowed direct comparison with experiment, with only one structure satisfying the requirement of being both energetically favorable and generating an STM simulation in agreement with experiment. This (4 × 2) phase possesses both prolate conformers in a 50:50 distribution, leading to an enantiopure overlayer with heterochiral adsorption footprints stabilized by strong one-dimensional hydrogen bonded chains. The identification of individual conformers and their adsorption footprints within an organized assembly represents an important step forward in the characterization of biomolecular monolayers at surfaces. Finally,

the single-molecule level insights afforded by this adsorbate make it highly promising for exploring the behavior of racemic systems and may provide important input toward understanding the complex behavior reported for racemic mixtures of amino acids adsorbed on metal surfaces.[12,14d]

Acknowledgment. R.R. and M.F. acknowledge the Engineering and Physical Sciences Research Council (EPSRC), the Biotechnology and Biological Sciences Research Council (BBSRC), and the University of Liverpool for equipment grants, funding, and a studentship for M.F. M.P. acknowledges the Swedish Research Council (VR) and the Marie Curie Research Training Network PRAIRIES, contract MRTN-CT-2006-035810. M.S.D. acknowledges the University of Liverpool for funding of a postdoctoral fellowship and computational resources.

Supporting Information Available: Table showing the full list of calculated frequencies, absolute RAIRS intensities, and description of the 70 normal modes of vibration possessing frequencies higher than 600 cm^{-1}. This material is available free of charge via the Internet at http://pubs.acs.org.

JA9020364